doi:10.2533/chimia.2013.142 Chimia 67 (2013) 142–148

Dye-sensitized Solar Cells Employing a SnO_2-TiO_2 Core-shell Structure Made by Atomic Layer Deposition

Martin Karlsson[a], Indrek Jõgi[a], Susanna K. Eriksson[a], Håkan Rensmo[b], Mats Boman[a], Gerrit Boschloo[a], and Anders Hagfeldt*[a]

Abstract: This paper describes the synthesis and characterization of core-shell structures, based on SnO_2 and TiO_2, for use in dye-sensitized solar cells (DSC). Atomic layer deposition is employed to control and vary the thickness of the TiO_2 shell. Increasing the TiO_2 shell thickness to 2 nm improved the device performance of liquid electrolyte-based DSC from 0.7% to 3.5%. The increase in efficiency originates from a higher open-circuit potential and a higher short-circuit current, as well as from an improvement in the electron lifetime. SnO_2-TiO_2 core-shell DSC devices retain their photovoltage in darkness for longer than 500 seconds, demonstrating that the electrons are contained in the core material. Finally core-shell structures were used for solid-state DSC applications using the hole transporting material 2,2',7,7',-tetrakis(N,N-di-p-methoxyphenyl-amine)-9,9',-spirofluorene. Similar improvements in device performance were obtained for solid-state DSC devices.

Keywords: Core-shell · Dye-sensitized solar cell · Electron lifetime · Photo-capacitor · Spiro-OMeTAD

1. Introduction

Dye-sensitized photoelectrochemical solar cells (DSC) based on high surface area titanium dioxide have attracted extensive academic and commercial research.[1] Most research has been devoted to the synthesis of new sensitizer molecules and to the photovoltaic characterization of titanium dioxide (TiO_2) based DSC devices.[2–5] Less attention has been given other classes of metal oxide semiconductors such as ZnO,[6–8] tin dioxide (SnO_2)[9,10] and Nb_2O_5[11,12] which all have, so far, given less efficiency than DSC based on a mesoporous network of TiO_2, which currently reaches efficiencies of 12%.[13] During operation of a DSC electrons are injected from a photo-excited dye into the metal oxide nanoparticle, from where they move through the mesoporous network by diffusion to the electron collecting contact. A redox mediator which diffuses to the counterelectrode where it is again reduced reduces the oxidized sensitizer. The mesoporous metal oxide electrode provides a large internal surface area on which the sensitizer dye can adsorb. It also provides, however, a large surface area at which electrons can recombine with oxidized sensitizer dye molecules or oxidized species in the electrolyte thus lowering the photocurrent of the solar cell. While the electron diffusion length, which is the average displacement length for an electron with a certain lifetime, in the TiO_2 and iodide/triiodide (I^-/I_3^-) system, is usually longer than the TiO_2 electrode thickness it might not be the case for other redox mediators or for solid-state DSC.[14–17] Thus, to limit the recombination current in DSC is one of the principal targets for increased device efficiency. Two main routes have been employed to decrease the recombination rate between electrons and holes, either by physically blocking the interface where the recombination occurs or by separating the charges in space using an energy gradient to draw charge away from the recombination interface.

The distinctions between the two methods are in the ways charges are conveyed through the material. In the first approach electrons must tunnel through the barrier while the second approach relies on electrons being conducted through the barrier. Examples of the first approach includes the synthesis of sensitizer dye molecules with blocking properties such as adding long alkoxy chains on the dye structure.[18–20] Another example is to apply an insulating material between the working electrode and the sensitizer dye molecule. This core-shell method has been successfully applied on TiO_2,[21,22] SnO_2,[23–25] and ZnO[26,27] using various materials such as MgO, ZrO_2, SiO_2 and Al_2O_3. Additives have also been used to suppress recombination in DSC either by chemisorbed species such as different phosphonic acids[28,29] or by physisorbed species such as the commonly used 4-*tert*-butyl pyridine[30] or chenodeoxycholic acid.[31] The application of a barrier layer often results in various penalties in the operation of the solar cell, such as reducing the photo-excited injection yield even when using very thin insulating metal oxide coatings.[26,32] Additives may displace sensitizing dye molecules with lower photocurrent as a result and might therefore not be a viable route for increasing DSC device performance.[33] One early example of introducing an energy gradient into the electron conducting material was realized by mixing SnO_2 and ZnO particles together, resulting in DSC devices with significantly higher photocurrents compared to the solar cells made from the pure material.[34] This procedure resulted in an ultrathin ZnO coating on the SnO_2 particles. Other authors have also published DSC core-shell structures using SnO_2 in conjunction with conductive metal oxide coatings.[23,35,36] Combining the two methods, using both a conductive and an insulating material coated on SnO_2 particles, has shown remarkable results in a solid-state DSC based on the hole transporting material 2,2',7,7',-tetrakis(N,N-di-p-methoxyphenyl-amine)-9,9',-spirofluorene (spiro-OMeTAD).[37] The popularity of using the SnO_2 particle as an electron transporting material for DSC stems from the higher electron bulk mobility seen in crystalline

*Correspondence: Prof. A. Hagfeldt[a]
E-mail: anders.hagfeldt@kemi.uu.se
[a]Department of Chemistry, Ångström Laboratory
Uppsala University
Box 523, 751 20 Uppsala, Sweden
[b]Condensed Matter Physics, Ångström Laboratory
Uppsala University
Box 516, 751 20 Uppsala, Sweden

SnO_2 (~100–200 cm^2 V s^{-1})[38] compared to crystalline TiO_2 (~0.1 cm^2 V s^{-1}).[39] The relevance of these values are questionable for DSC application where electrons have to travel over μm thicknesses of interconnected nanoparticles and where it is common to see slower transport in SnO_2 than for TiO_2.[9,40] Most of the deposition methods for creating these core-shell structures in DSC are very simple, either by mixing the colloid with a solution of the dissolved metal ion[23] or by a dip coating technique where the sintered mesoporous working electrode is submersed in a solution of the coating metal ion.[37,41] These rather coarse deposition methods might yield non-uniform coatings with pin-holes or with areas not coated at all.

Atomic layer deposition (ALD) is a powerful technique for depositing conformal coatings on high aspect ratio materials such as mesoporous metal oxide films.[42] We have employed the ALD technique to coat mesoporous SnO_2 films with layers of TiO_2 for application in both liquid and solid-state electrolyte DSC. The aim of this paper is to present a solar cell which uses a core material as an electron sink while it also transports charges to the collecting electrode. The shell material should act like a barrier for electron recombination from the core but still allow electron injection from the photo-excited dye. As sensitizer we use the dye D35 which has proven to work efficiently in both the liquid and solid-state system.[43] To the best of our knowledge this is the first time a structure made by the ALD technique using a SnO_2-TiO_2 core-shell has been presented.

2. Material and Methods

2.1 *Preparation of SnO_2 Nanoparticles and Printing Paste*

Rod-like SnO_2 particles (8 × 20 nm) were prepared through a basic synthetic route. $Sn(IV)Cl_4{\cdot}5H_2O$ was dissolved in 2-propanol and added dropwise under stirring to a saturated NaOH solution in 2-propanol. A precipitate was formed and the sol was refluxed for 8 h, followed by a thermal autoclaving step for 12 h at 220 °C (380 psi). The resulting colloidal suspension was washed 3 times by precipitating the colloids by centrifugation, decanting the supernatant and re-dispersing the solid in ethanol. This step was done to remove chloride salts. The ethanol was exchanged to α-terpineol solvent and ethyl cellulose was added as a binder to the final paste.

2.2 *Solar Cell Preparation*

Dye-sensitized solar cells were prepared on fluorine-doped tin oxide glass substrates (Pilkington-TEC15) which had been cleaned in an ultra-sonic bath with detergents, acetone and ethanol. For the solid-state DSC a 30 nm metallic tin layer was evaporated through resistive heating of a tungsten boat filled with tin metal under reduced pressure (10^{-6} mbar). The metallic film was heated to 450 °C (for 45 min) to oxidize the metal to form SnO_2 under layers. The mesoporous SnO_2 working electrode was deposited by multiple doctor-blading steps for the liquid electrolyte DSC and by a single spin-coating step for the solid-state DSC, followed by a 45 min, 450 °C, sintering step (with a ramping time of 30 min from room temperature). The working electrode thickness was measured using a profilometer. The finished mesoporous SnO_2 working electrodes were coated with TiO_2 by an ALD technique as described in the separate section below. After this step the SnO_2-TiO_2 core-shell working electrodes were stored and re-conditioned by sintering before use. The dye bath solution contained 0.2 mM D35 dissolved in ethanol and each dye bath was only used once.[43] The working electrodes were submersed warm into the dye bath and kept for 12 h before taken up and rinsed with ethanol to remove non-chemically attached dye molecules. The assembly of the liquid electrolyte DSC continued by melting the platinized counter electrode together with the dyed working electrode using a thermoplastic foil (Surlyn, DuPont). The electrolyte was introduced into the liquid electrolyte solar through holes drilled in the counter electrode which were subsequently sealed with a new layer of glass and Surlyn. The electrolyte composition was as followed: 0.03 M I_2, 0.6 M 1-hexyl-3-methylimidazol iodide, 0.1 M guanidinium thiocyanate and 0.5 M 4-*tert.*-butylpyridine (t-BP) in a 50:50 solution of acetonitrile and valeronitrile. The hole transporting material for the solid-state DSC was prepared by dissolving 2,2',7,7',-tetrakis(N,N-di-p-methoxyphenyl-amine)-9,9',-spirofluorene in chlorobenzene and then adding t-BP also dissolved in chlorobenzene. A solution of $Li[(CF_3SO_2)_2N]$ in acetonitrile was added to the spiro-OMeTAD/tBP mixture, yielding a final solution containing 0.12 M spiro-OMeTAD, 0.06 M tBP and 0.015 M Li-salt in a 95:5 solvent mixture of chlorobenzene and acetonitrile. The hole transporting mixture was applied to the dyed working electrode by spin-coating at 2000 rpm for 30 seconds. The solid-state DSC was completed by thermally evaporation of a 100 nm thick silver contact on top of the over-standing spiro-OMeTAD layer.

2.3 *Preparing Working Electrodes with Atomic Layer Deposition*

TiO_2 coatings were prepared in a flow-type atomic layer deposition reactor (Picosun R150). The films were prepared at 2.5 hPa pressure with nitrogen used as carrier and purging gas. $TiCl_4$ and H_2O were used respectively as Ti and O precursors. Experiments were carried out with a $TiCl_4$ pulse length of 2 s and H_2O pulse of 5 s. Increasing the $TiCl_4$ dosing time to 5 s resulted in peeling of the SnO_2 electrodes after 40 treatment cycles and was attributed to the effect of $TiCl_4$. Due to the highly porous surfaces of the SnO_2 electrodes, relatively long purge periods of 25 s were used. The electrodes of SnO_2 were kept at 300 °C during deposition of TiO_2.

2.4 *Solar Cell Measurements*

The current–voltage characteristics of both the liquid electrolyte and solid-state DSC devices were measured using a 300 W solar simulator (Newport 91160), calibrated to 1000 W m^{-2} with an irradiance comparable with the 1.5 AM Global spectral distribution. The calibration value was assured by using a certified IR-filtered Si solar cell (Fraunhofer ISE). The current density–voltage data was recorded on a computer-controlled digital sourcemeter (Keithley, Model 2400). The active area of the device was 0.25 cm^2 for the liquid electrolyte DSC and 0.2 cm^2 for the solid-state DSC. The DSC devices were masked to an aperture area of 0.36 cm^2 and 0.3 cm^2, respectively. Incident-photon-to-current-conversion-efficiency (IPCE) measurements were carried out by reading the difference in photo-current when a monochromatic light was superimposed with a frequency of 10 Hz on top of a white LED light with an intensity of approximately 1000 W m^{-2}.

2.5 *Electron Lifetime, Charge Extraction and Voc Decay Measurements*

The electron lifetime was measured on complete liquid electrolyte DSC devices by applying a small square-wave light modulation on top of a background white light LED. By measuring the transient change in the open-circuit potential of the solar cell with the light modulation it is possible to obtain the electron lifetime of the device. Charge extraction measurements were performed in the following way: the solar cell was illuminated for 5 s at open-circuit conditions at ~1000 W m^{-2}. At the same time as the light source is turned off the external circuit is short-circuited and the current density is read out and integrated over time. The integrated charge density is proportional to the initial V_{OC} value of the device. The V_{OC} decay measurement is performed in a similar way to the electron lifetime measurement but instead of using a small square-wave modulation the V_{OC} decay technique uses an on-off light source. The solar cell is kept under 1000 W m^{-2} illumination and at open-circuit conditions

for 10 s. The light is then turned off and the V_{OC} is measured as a function of time.

2.6 *Material Characterization*

Samples for powder X-ray diffraction (XRD) were prepared by sintering a part of the colloidal SnO_2 paste, at 450 °C for 45 min, and grinding the resulting solid to a fine powder in a solution of ethanol. The suspension was spread on a glass substrate and left to dry. The diffractogram was recorded using CuKα radiation from a Siemens D5000 (2-Φ) diffractometer. Samples for the transmission electron microscopy (TEM) were prepared by removing the solid film of the working electrode, both with and without ALD treatment, from the substrate. The solid samples were dispersed in ethanol and ground in a mortar before they were dropped on the TEM grid. The TEM pictures were taken on a FEI Titan 300 transmission electron microscope (300 keV). Beam damage could be observed for the core-shell particles and care was taken to avoid it and not to analyze any pictures containing traces of beam damage.

The photoelectron spectroscopy (PES) measurements at high kinetic energy were performed using hard X-ray synchrotron light at the high kinetic energy electron spectroscopy (HIKE or HAXPES) end station on the beamline KMC-1 at BESSY in Berlin.[44] The different peaks were measured using photon energy of 2010 eV leading to a kinetic energy for O *1s*, Sn *3d* and Ti 2*p* around 1500 eV. To estimate the TiO_2 thickness the peak intensities for Ti 2*p* and Sn 3*d* were first compared to assess how much in relative numbers the thickness of the TiO_2 layer were increased with increased number of ALD cycles. A constant amount of oxygen in both the SnO_2 and TiO_2 phase was assumed to normalize the photon flux and based on this assumption the intensities (areas) of the Sn *3d* relative to the O *1s* peaks was used to calculate the TiO_2 coating thickness (see below).

3. Results and Discussion

The prepared SnO_2 paste was calcined at 450 °C and ground to a powder, which was used to determine the crystal structure by means of powder X-ray diffraction (XRD). The diffraction peaks corresponded to the tetragonal rutile structure of SnO_2, the casserite structure (Fig. 1). The XRD of the thickest TiO_2 coated sample did not show any additional diffraction peaks, indicating an amorphous TiO_2 shell. The size and dimension of both the pure SnO_2 and the coated SnO_2 particle were determined by transmission electron microscopy (TEM). Fig. 2a shows the typical elongated shape of the pure SnO_2 particle, a shape which has previously been described to have its (110) rutile plane along the length of the particle.[45,46] Films of these SnO_2 particles were coated with TiO_2 using the ALD technique as described below.

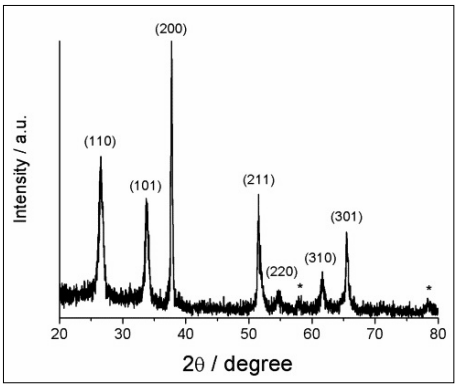

Fig. 1. The XRD pattern recorded for SnO_2 colloidal paste which has been sintered at 450 °C. The diffractogram peak corresponds to the tetragonal rutile structure of SnO_2 very similar to that presented in JCPDS 21-1250. The * correspond to (112) at 57.5° and (321) at 78°.

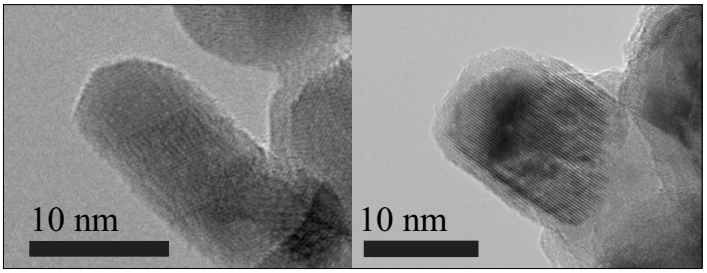

Fig. 2. Transmission electron microscope (TEM) picture depicting a typical pure SnO_2 particle, prepared as described in the experimental section (left). A SnO_2 particle coated through 40 ALD cycles with TiO_2 (right).

Samples were treated with 10, 20, 30 or 40 ALD cycles. Increasing the TiO_2 coating to more than 40 cycles resulted in SnO_2 films where the active areas started to peel off from the transparent conductive metal oxide (TCO) substrate. The reason for this was not further investigated, but it is believed to be due to the acidic properties of the ALD precursor, titanium tetrachloride ($TiCl_4$). Fig. 2b shows a typical SnO_2 particle which has been coated with 40 cycles of TiO_2 ALD treatment. It is possible to discern an outer, lighter grey shell on top of the darker core of the particle. The gradient between light and dark grey in each individual TEM picture corresponds to the gradient of electron transmission through the sample. The heavier material SnO_2 (6.85 g cm^{-3}) would be expected to have a darker grey color compared to the lighter material TiO_2 (4.23 g cm^{-3}), yielding a TEM picture with a dark core and a lighter shell around it.[47] The width of the SnO_2 core in Fig. 2b is approximately 9 nm, slightly larger than the average width, while the total width of the particle is approximately 12 nm, yielding a total TiO_2 shell thickness of 3 nm. Due to the size distribution of the SnO_2 particles and the difficulty to determine the TiO_2 shell thickness for the different ALD cycles it is more relevant to report the average particle width as a function of the number of TiO_2 ALD cycles, as seen in Fig. 3. The average width of pure SnO_2 particles was determined to be 8.3 ± 1.4 nm with the median particle width slightly lower (7.9 nm). The standard deviation was increasing with number of ALD cycles mainly because some few SnO_2 particles seemed to be only partly covered with TiO_2. A partial TiO_2 coating is expected as a consequence of the particle to particle necking, leaving some SnO_2 surface area not exposed to the ALD treatment.

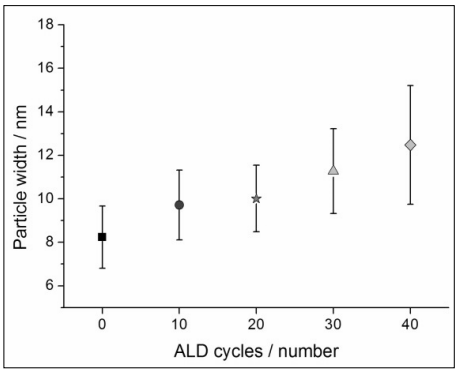

Fig. 3. Dependence of the average width of the particle (the width of the SnO_2 core plus the thickness of the TiO_2 shell) with the numbers of ALD cycles. The thickness was estimated with a resolution of 0.5 nm and the average width and the standard deviation (error bar) were determined from more than 40 particles per ALD cycle.

A linear fit to the data in Fig. 3 yields a slope of 0.1 nm per ALD cycle which is below one atomic monolayer per ALD cycle, a common observation for ALD coatings.[48] The ALD growth rate of TiO_2 from titanium isopropoxide and temperature between 150–250 °C with water as an oxygen source has previously been reported to be in the range of 0.05–0.15 nm per ALD cycle, very similar to the results presented here.[48] To investigate the elemental composition of the core-shell structure photoelectron spectroscopy (PES) was employed. PES is a surface sensitive technique well suited for quantitative determination of different elements. Fig. 4 (top) shows how the signal ratio between the normalized integrated areas of the Sn *3d* peak over the O *1s* peak

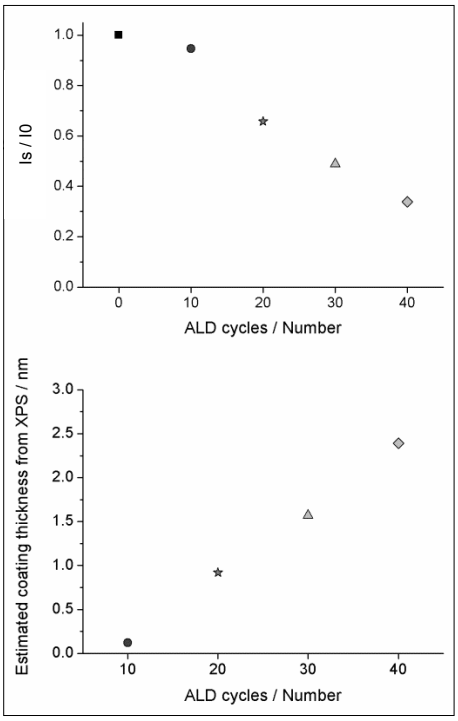

Fig. 4. The dampening of the Sn *3d* signal from the core-shell structure as determined by PES with changes in the number of ALD cycles (top). The thickness of the TiO_2 coating is estimated from the attenuation of the Sn *3d* PES signal (bottom).

changes when increasing the numbers of TiO_2 ALD cycles coated on the SnO_2 particles. As expected, the titanium signal increases with increasing number of ALD cycles, indicating a thicker TiO_2 coating with increased number of ALD cycles, consistent with the findings from the TEM study above.

Using the PES intensities it is possible to estimate the coating thickness of the different TiO_2 layers from the attenuation of the Sn 3*d* signal. The inelastic mean free path is a measure of the probability for inelastic scattering and is material and kinetic energy dependent.[49] The lower y-axis of Fig. 4 shows the estimated TiO_2 coating thickness according to the equation of the inelastic mean free path of a photoelectron (Eqn. (1))

$$\frac{I_s}{I_0} = \exp\left(\frac{-d}{\lambda}\right) \quad (1)$$

where I_0 is the Sn signal intensity of pure SnO_2 and I_s is the Sn signal intensity of the sample under evaluation. λ is the value of the inelastic mean free path (IMFP) and is chosen to be 2.2 nm taken from literature at 1500 eV kinetic energy.[50] When comparing the estimation of the TiO_2 thickness from the PES measurement with the average particle width of Fig. 3 it is important to note that TEM measurements represent the diameter of the particle while

Table 1. Solar cell parameters for SnO_2-TiO_2 core-shell DSC built with different coating thickness of TiO_2.

Name[a]	V_{OC} [mV]	J_{SC} [mA cm^{-2}]	Fill factor [%]	Efficiency [%]
SnO_2	335	6.1	36	0.73
SnO_2 + 10c	625	6.7	49	2.07
SnO_2 + 20c	660	6.9	54	2.48
SnO_2 + 30c	690	8.3	52	2.97
SnO_2 + 40c	710	8.9	55	3.47

[a]Active area of the devices was 0.25 cm^2 and all measurements were done at 1000 W m^{-2}. Number of TiO_2 ALD cycles (c) is indicated.

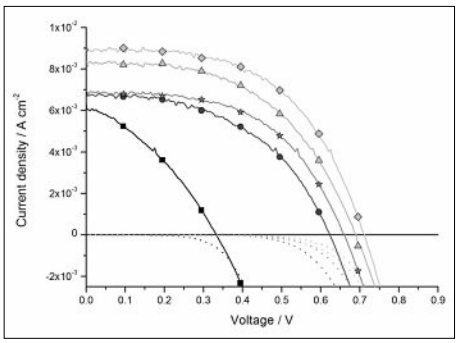

Fig. 5. J-V curves of SnO_2-TiO_2 core-shell liquid electrolyte DSC with D35 as sensitizer. Pure SnO_2 electrode (black square), SnO_2 + 10 cycle TiO_2 (dark grey circle), SnO_2 + 20 cycle TiO_2 (grey star), SnO_2 + 30 cycle TiO_2 (light grey pyramid) and SnO_2 + 40 cycle TiO_2 (light grey diamond). All samples were illuminated by 1000 W m^{-2} with AM1.5G spectral distribution.

XPS values only correspond to the coating thickness. For the 40 cycles TiO_2 ALD coating, TEM suggests a coating thickness around 2 nm while the estimation obtained from XPS measurements imply a coating thickness of 2.4 nm. The working electrode for liquid electrolyte DSC was prepared by doctor-blading with thickness of ~10 μm. After coating the substrates with TiO_2 through the ALD technique the working electrodes were assembled into solar cell devices. For a more complete description of the solar cell preparation please refer to the experimental section. Fig. 5 shows the current density–voltage characteristics of the liquid electrolyte DSC based on SnO_2 particles coated with TiO_2. It is apparent that all solar cell parameters are influenced when changing the TiO_2 coating thickness on the SnO_2 particle. Table 1 shows the complete comparison, in solar cell device parameters, between the different core-shell thicknesses. There is a significant increase in solar energy conversion efficiency from 0.7% for the pure SnO_2 particles to 3.5% for the core-shell structure prepared with 40 cycles of TiO_2 ALD treatment. The increase in performance with increasing thickness is due to a higher short-circuit current density (J_{SC}) and a higher fill factor (FF) but also due to a higher open-circuit potential (V_{OC}) of the device.

These values should be compared to previous work where the TiO_2 coating was deposited using techniques other than ALD. Kay and Grätzel treated a SnO_2 colloid with a $TiCl_4$ solution to form an ultrathin TiO_2 shell, which reached a solar cell efficiency of 3.9% in combination with the sensitizing dye N719.[23] Qian *et al.* prepared multilayer hollow SnO_2 microspheres using wet chemical methods that reached efficiencies of 5.65% with N716 after aqueous $TiCl_4$ treatment.[35] The extinction coefficient for D35 is 31.3·10^3 M^{-1} cm^{-1} at the absorption maximum, 500 nm.[43] The high extinction coefficient of the dye together with the thickness of the electrode assured that almost all photons, with energy close to that of the absorption maximum of the dye, are absorbed by the dye. Fig. 6 shows the incident-photon-to-current conversion efficiency (IPCE) of the DSC devices made with different thicknesses of TiO_2 coating. The trend in photo-current seen in Table 1 is well reflected in the improvement of IPCE with the number of ALD cycles. The highest IPCE value for pure SnO_2 particles is 45% at 450 nm, a value which increases to over 60% for SnO_2 particles with 40 cycles of TiO_2 ALD treatment. The increase in IPCE when applying a TiO_2 coating on the SnO_2 particle can be attributed to either better light harvesting efficiency, higher charge collection efficiency, higher electron injec-

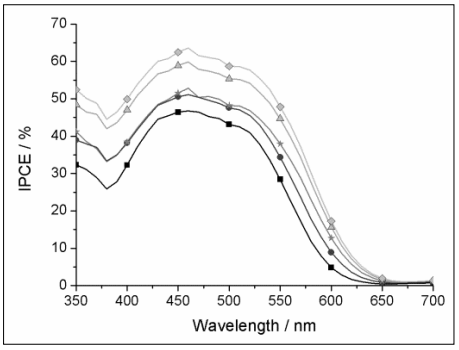

Fig. 6. IPCE of DSC devices made with the sensitizer dye D35. Pure SnO_2 electrode (black square), SnO_2 + 10 cycles TiO_2 (dark grey circle), SnO_2 + 20 cycles TiO_2 (grey star), SnO_2 + 30 cycles TiO_2 (light grey pyramid) and SnO_2 + 40 cycles TiO_2 (light grey diamond).

tion efficiency or to a slower back-reaction of metal oxide electrons with oxidized dye molecules.

The light harvesting efficiency of D35 on SnO_2 particle is already very high, especially around 450–500 nm, with little room for improvement when adding TiO_2 shells. In the absence of ultra-fast spectroscopic evidence it is hard to draw any conclusions about the difference in electron injection dynamic of D35 on pure SnO_2 particles compared to SnO_2-TiO_2 core-shell structures. Comparative studies of electron injection rates for organic sensitizing molecules between different metal oxides are scarce, but the same comparison for ruthenium complexes exists. The ruthenium complex, Z907, has for example a slower electron injection rate from the dye to SnO_2 than to TiO_2.[40] The rate of electron injection depends not only on the driving force for injection but also on the electronic coupling between the semiconductor and dye, the amount of acceptor states in the semiconductor, dye loading and the binding mode of the dye.[51,52] Many of the parameters influencing the electron injection yield are dependent on the direct interface between the semiconductor and the dye. The increase in photocurrent seen in Fig. 6 might be a gradual effect from modifying the pure SnO_2 particle, with a relatively slow electron injection rate, to a TiO_2 surface having a good electronic coupling between the semiconductor and dye giving good injection yields. It is possible that an increase in charge collection efficiency also plays a role in the improvement in photo-current seen in Fig. 6. The electron lifetime is measured under different light intensities yielding different V_{OC}. At V_{OC} the quasi-Fermi level (QFL) is constant throughout the metal oxide film and the charge density in the film is high.[53] At short-circuit the QFL is generally lower and shows a gradient and thus the charge density is lower compared to open-circuit conditions. By measuring the amount of charges present in each device at different light intensity and at both short-circuit and open-circuit conditions it is possible to relate the electron lifetime and the electron transport time to the amount of stored charges in the metal oxide film. Fig. 7 shows the electron lifetime and electron transport time and how they depend on the amount of charges stored in the DSC device. The apparent electron diffusion coefficient can be estimated from Eqn. (2):

$$L_D = \sqrt{(\tau_e D_e)} \qquad (2)$$

where L_D is the apparent electron diffusion length, τ_e the electron lifetime and D_e the electron diffusion coefficient. The electron diffusion coefficient for the ALD-coated

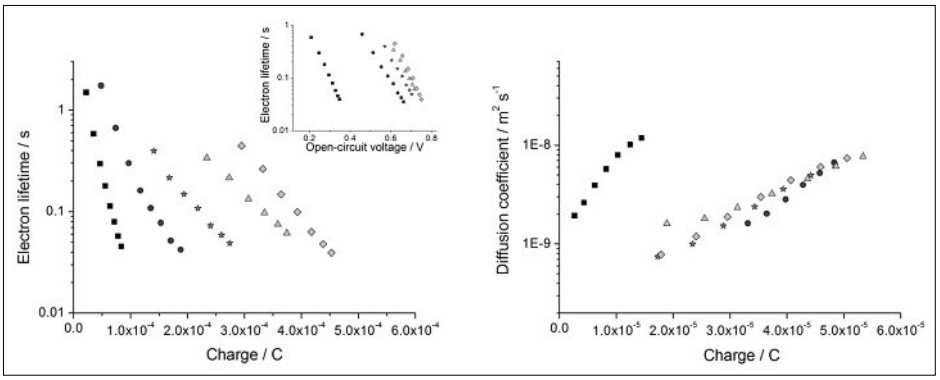

Fig. 7. Electron lifetime of DSC versus extracted charge when switching the device from open-circuit potential to short-circuit (a, left) and the electron diffusion coefficient of DSC versus the extracted charge at short-circuit (b, right). The inset of Fig. 7a shows the electron lifetime versus the measured open-circuit voltage. Pure SnO_2 electrode (black square), SnO_2 + 10 cycles TiO_2 (dark grey circle), SnO_2 + 20 cycles TiO_2 (grey star), SnO_2 + 30 cycle TiO_2 (light grey pyramid) and SnO_2 + 40 cycle TiO_2 (light grey diamond).

SnO_2 particles is very similar regardless of number of TiO_2 ALD cycles but is significantly slower than the pure SnO_2 material and even slower than pure TiO_2. This effect might be accounted for by a less efficient screening of charge carriers within the SnO_2 material, by ions in the electrolyte, when there is a coating present. The transport might also be affected by the formation of extra traps at the SnO_2-TiO_2 interface, for example from the lattice mismatch between the rutile SnO_2 and the TiO_2, where extra traps will slow down the electron diffusion. The apparent electron diffusion length for the pure SnO_2 electrode was determined to be 13.5 μm under 1000 W m^{-2} illumination. The similarity of the electron diffusion length with the actual thickness of the DSC devices based on pure SnO_2 (10 μm) indicates that there are significant recombination losses occurring even under short-circuit conditions. Increasing the number of TiO_2 ALD cycles from 10 to 40 yields DSC devices which are capable of storing more charges at open-circuit potential while keeping the electron diffusion coefficient constant, with the result that the apparent electron diffusion length increases by several orders of magnitude.

The shift of the lifetime curves in Fig. 7a with increasing thickness of the TiO_2 shell indicates that the barrier property of the conformal TiO_2 coating on the SnO_2 is effective. The TiO_2 coating suppresses the leakage of electrons from the conduction band of the SnO_2 to the electrolyte to such extent that the open-circuit potential of the DSC device with 40 cycles TiO_2 ALD coating is more than doubled from that of the pure SnO_2 material. The increase in photovoltage of the device can come from two sources; either from an increase of the conduction band of the SnO_2/TiO_2 material or from the accumulation of charges inside the metal oxide semiconductor by suppressing the dark current.[22,54] Charge extraction measurements suggest that the conduction band shift is between 100 mV to 150 mV for the core-shell material (Fig. 8), demonstrating that the increase in electron lifetime is the main cause for large V_{OC}. A combination of these two effects has previously been proposed to explain the increase in V_{OC} for SnO_2-TiO_2 core-shell structures.[41] We note that the combination of the electron storing capacity of the core-shell material together with the exceptionally long electron lifetime could also form the basis of a self-charging photo-capacitor.[55] Fig. 9 shows the V_{oc} decay of the different TiO_2 coatings and how the conformal SnO_2-TiO_2 core-shell structure retains the photovoltage over long periods of time. For the thickest TiO_2 coating of 40 cycles the photovoltage is retained well over 500 seconds, showing the slow recombination dynamics between the electrons in metal oxide and the redox electrolyte. The slow recombination is a strong indication that electrons are transferred from the outer TiO_2 shell to the inner SnO_2 core. The bi-exponential decay from a fast

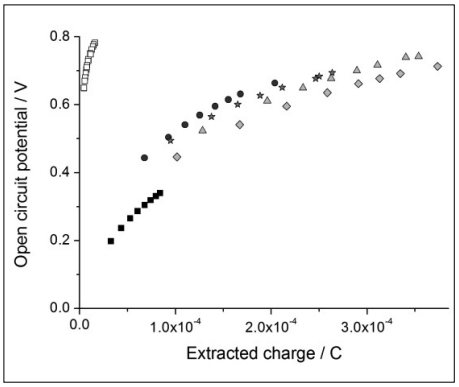

Fig. 8. Charge extraction measurement of DSC with different amount of TiO_2 ALD coating on the SnO_2 particles. Pure SnO_2 electrode (black square) and pure TiO_2 (open squares). SnO_2 + 10 cycle TiO_2 (dark grey circle), SnO_2 + 20 cycle TiO_2 (grey star), SnO_2 + 30 cycle TiO_2 (light grey pyramid) and SnO_2 + 40 cycle TiO_2 (light grey diamond).

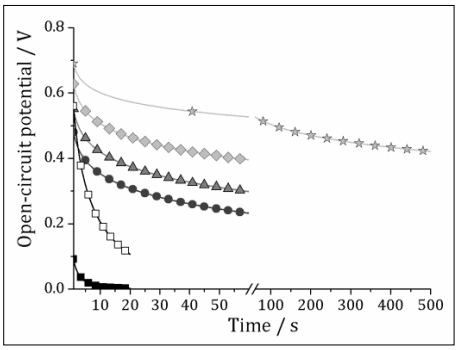

Fig. 9. V_{OC} decay measurement of DSC with different amount of TiO_2 ALD coating on the SnO_2 particles. The 40 cycles TiO_2 ALD is recorded until 500 seconds as seen on the extended scale. Pure SnO_2 electrode (black square), SnO_2 + 10 cycle TiO_2 (dark grey circle), SnO_2 + 20 cycle TiO_2 (grey star), SnO_2 + 30 cycle TiO_2 (light grey pyramid) and SnO_2 + 40 cycle TiO_2 (light grey diamond). All samples were charged by illuminating the device at 1000 W m^{-2} for 10 seconds before the V_{OC} decay measurement commenced.

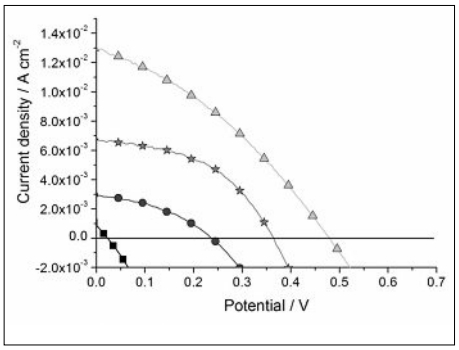

Fig. 10. J-V curves of a solid-state DSC based on the sensitizer dye D35 and spiro-OMeTAD. Pure SnO_2 electrode (black square), SnO_2 + 10 cycles TiO_2 (dark grey circle), SnO_2 + 20 cycles TiO_2 (grey star), SnO_2 and 30 cycles TiO_2 (light grey pyramid). Illumination intensity: 1000 W m^{-2} with AM1.5G spectral distribution.

and a slow component of the open-circuit potential is seen both for DSC devices made from pure SnO_2 materials as well as the core-shell structures. The difference in rate constants between the pure SnO_2 material and the core-shell device lies in the slow component of the recombination process, being approximately one order of magnitude slower for the core-shell device compared to the pure material.

One of the main drawbacks with using solid-state hole transporting materials such as spiro-OMeTAD is that they have a much faster electron recombination dynamics compared to liquid electrolyte DSC based on I^-/I_3^- electrolyte.[56] The sharp reduction in the apparent electron diffusion length at applied potential keeps the overall solid-state device efficiency lower than that of its liquid electrolyte counterpart.[57] Therefore it is very interesting to apply these SnO_2-TiO_2 core-shell structures in a solid-state DSC device made from spiro-OMeTAD. In order to get functioning solid-state devices it is critical to form a blocking layer between the FTO contact and the mesoporous SnO_2 working electrode and the hole transporting material interface. This is usually done by a spray pyrolysis method in solid-state DSC devices made with TiO_2 working electrodes. Here we form underlayers for SnO_2 based solid-state DSC by evaporation of tin metal on the FTO substrate followed by heating in air to oxidize the metal. Fig. 10 shows J-V curves of solid-state DSC based on thin working electrodes of SnO_2 (1.6 +/–0.1 μm) coated with different numbers of ALD cycles of TiO_2. A very similar trend in the increase of conversion efficiency is seen for solid-state DSC as is seen for its liquid electrolyte counterpart. Interestingly, as could be seen in Fig. 10, the pure SnO_2 working electrode does not work at all in the solid-state DSC configuration. When the SnO_2 electrode is coated with 10, 20 and 30 cycles of TiO_2 ALD treatments the conversion efficiency is increased from 0.3%, 1.2% to 2.1%. The solid-state DSC based on SnO_2 with 40 cycles of TiO_2 ALD coating shows very high short-circuit current densities of almost 13 mA/cm^2. We note that the J_{SC} value is probably slightly too high for D35 measured under simulated AM1.5 given the absorption spectrum of this dye.[43] This could be due to improper masking of the device using an aperture area larger than the device area, 0.3 cm^2 and 0.2 cm^2 respectively.[58] Light piping effects may therefore slightly overestimate the J_{SC} value reported here. The increase of V_{OC} seen in Fig. 10 with increasing thickness of TiO_2 coating is similar to that in Fig. 5 with the difference that the change in V_{OC} is larger for solid-state DSC than for liquid electrolyte DSC.

4. Conclusion

Atomic layer deposition is a powerful tool in controlling core-shell mesoporous electrodes for dye-sensitized solar cells. Previously, an increase in electron lifetimes has been observed when employing core-shell structures based on wide band gap semiconductor cores and insulating shell materials. The drawback with this method is the reduction in electron injection when increasing the shell thickness. This problem may be solved by choosing two wide band gap semiconducting materials, in such a manner that photogenerated electrons can be both injected and move from the outer shell material to the inner core material of the working electrode. We have demonstrated a system where a SnO_2 core material acts like an electron drain on the TiO_2 shell material, increasing the electron lifetime with increasing thickness of the TiO_2 shell coating. Utilizing the unique control over coating thickness that the ALD technique offers we have shown that solar cell parameters, such as J_{SC} and V_{OC}, increase with coating thickness of the shell material, with no indications of a reduction in electron injection yield. Using this method we have built liquid electrolyte DSC devices which are able to store photogenerated charges for more than 500 seconds, creating a self-charging photocapacitor. These SnO_2-TiO_2 core-shell structures have also been found to increase the efficiency of solid-state DSC based on spiro-OMeTAD and might be a viable route to increase the conversion efficiency of these devices even further.

Acknowledgements

We thank BASF SE, the Bundesministerium für Bildung and Forschung (BMBF), the Swedish Energy Agency, the Swedish Research Council, and the STandUP for Energy program for financial support.

Received: February 4, 2013

[1] B. O'Regan, M. Grätzel, *Nature* **1991**, *353*, 737.
[2] M. K. Nazeeruddin, S. M. Zakeeruddin, J.-J. Lagref, P. Liska, P. Comte, C. Barolo, G. Viscardi, K. Schenk, M. Graetzel, *Coord. Chem. Rev.* **2004**, *248*, 1317.
[3] A. Mishra, M. K. R. Fischer, P. Bäuerle, *Angew. Chem. Int., Ed.* **2009**, *48*, 2474.
[4] A. Hagfeldt, G. Boschloo, L. Sun, L. Kloo, H. Pettersson, *Chem. Rev.* **2010**, *110*, 6596.
[5] J. M. Kroon, N. J. Bakker, H. J. P. Smit, P. Liska, K. R. Thampi, P. Wang, S. M. Zakeeruddin, M. Grätzel, A. Hinsch, S. Hore, U. Würfel, R. Sastrawan, J. R. Durrant, E. Palomares, H. Pettersson, T. Gruszecki, J. Walter, K. Skupien, G. E. Tulloch, *Prog. Photovolt: Res. Appl.* **2007**, *15*, 1.
[6] Q. Zhang, T. P. Chou, B. Russo, S. A. Jenekhe, G. Cao, *Angew. Chem. Int., Ed.* **2008**, *47*, 2402.
[7] W. J. Lee, A. Suzuki, K. Imaeda, H. Okada, A. Wakahara, A. Yoshida, *Jpn, J. Appl. Phys.* **2004**, *43*, 152.
[8] H. Rensmo, K. Keis, H. Lindström, S. Södergren, A. Solbrand, A. Hagfeldt, S.-E. Lindquist, L. N. Wang, M. Muhammed, *J. Phys. Chem.* **1997**, *101*, 2598.
[9] Y. Fukai, Y. Kondo, S. Mori, E. Suzuki, *Electrochem. Commun.* **2007**, *9*, 1439.
[10] I. Bedja, S. Hotchandani, P. V. Kamat, *J. Phys. Chem.* **1994**, *98*, 4133.
[11] P. Guo, M. A. Aegerter, *Thin Solid Films* **1999**, *351*, 290.
[12] L. Hu, M. Wolf, M. Grätzel, Z. Jiang, *J. Sol-Gel Sci. Technol.* **1995**, *5*, 219.
[13] A. Yella, H.-W. Lee, H. N. Tsao, C. Yi, A. K. Chandiran, M. K. Nazeeruddin, E. W.-G. Diau, C.-Y. Yeh, S. M. Zakeeruddin, M. Grätzel, *Science* **2011**, *334*, 629.
[14] H. K. Dunn, P.-O. Westin, D. R. Staff, L. M. Peter, A. B. Walker, G. Boschloo, A. Hagfeldt, *J. Phys. Chem. C* **2011**, *115*, 13932.
[15] Q. Yu, Y. Wang, Z. Yi, N. Zu, J. Zhang, P. Wang, *ACS Nano* **2010**, *4*, 6032.
[16] H. K. Dunn, L. M. Peter, *J. Phys. Chem. C* **2009**, *113*, 4726.
[17] M. Wang, P. Chen, R. Humphry-Baker, S. M. Zakeeruddin, M. Grätzel, *Chem. Phys. Chem.* **2009**, *10*, 290.

[18] K. M. Karlsson, X. Jiang, S. K. Eriksson, E. Gabrielsson, H. Rensmo, A. Hagfeldt, L. Sun, *Chem. Eur. J.* **2011**, *17*, 6415.
[19] P. Wang, S. M. Zakeeruddin, J. E. Moser, M. K. Nazeeruddin, T. Sekiguchi, M. Grätzel, *Nature Mater.* **2003**, *2,* 402.
[20] J. E. Kroeze, N. Hirata, S. Koops, M. K. Nazeeruddin, L. Schmidt-Mende, M. Grätzel, J. R. Durrant, *J. Am. Chem. Soc.* **2006**, *128*, 16376.
[21] E. Palomares, J. N. Clifford, S. A. Haque, T. Lutz, J. R. Durrant, *J. Am. Chem. Soc.* **2003**, *125*, 475.
[22] Y. Diamant, S. Chappel, S. G. Chen, O. Melamed, A. Zaban, *Coord. Chem. Rev.* **2004**, *248*, 1271.
[23] A. Kay, M. Grätzel, *Chem. Mater.* **2002**, *14*, 2930.
[24] C. Prasittichai, J. T. Hupp, *J. Phys. Chem. Lett.* **2010**, *1*, 1611.
[25] M. K. I. Senevirathna, P. Pitigala, E. V. A. Premalal, K. Tennakone, G. R. A. Kumara, A. Konno, *Sol. Energy Mater. Sol. Cells* **2007**, *91*, 544.
[26] M. Law, L. E. Greene, A. Radenovic, T. Kuykendall, J. Liphardt, P. Yang, *J. Phys. Chem. B* **2006**, 110, 22652.
[27] Y.-J. Shin, J.-H. Lee, J.-H. Park, N.-G. Park, *Chem. Lett.* **2007**, *36*, 1506.
[28] A. Allegrucci, N. A. Lewcenko, A. J. Mozer, L. Dennany, P. Wagner, D. L. Officer, K. Sunahara, S. Mori, L. Spiccia, *Energy Environ. Sci.* **2009**, *2*, 1069.
[29] P. Wang, S. M. Zakeeruddin, R. Humphry-Baker, J. E. Moser, M. Grätzel, *Adv. Mater.* **2003**, *15,* 2101.
[30] M. Dürr, A. Yasuda, G. Nelles, *Appl. Phys. Lett.* **2006**, *89*, 061110.
[31] T. Marinado, M. Halin, X. Jiang, M. Quintana, E. M. J. Johansson, E. Gabrielsson, S. Plogmaker, D. P. Hagberg, G. Boschloo, S. M. Zakeeruddin, M. Grätzel, H. Siegbahn, L. Sun, A. Hagfeldt, H. Rensmo, *J. Phys. Chem. C* **2010**, *114*, 11903.
[32] T. W. Hamann, O. K. Farha, J. T. Hupp, *J. Phys. Chem. C* **2008**, *112*, 19756.
[33] X. Jiang, T. Marinado, E. Gabrielsson, D. P. Hagberg, L. Sun, A. Hagfeldt, *J. Phys. Chem. C* **2010**, *114*, 2799.
[34] K. Tennakone, G. R. R. A. Kumara, I. R. M. Kottegoda, V. P. S. Perera, *Chem. Commun.* **1999**, 15.
[35] J. Qian, P. Liu, Y. Xiao, Y. Jiang, Y. Cao, X. Ai, H. Yang, *Adv. Mater.* **2009**, *21*, 3663.
[36] E. Joanni, R. Savu, M. de Sousa Góes, P. R. Bueno, J. Nei de Freitas, A. F. Nogueria, E. Longo, J. A. Varela, *Scr. Mater.* **2007**, *57*, 277.
[37] H. J. Snaith, C. Ducati, *Nano Lett.* **2010**, *10*, 1259.
[38] C. G. Fonstad, R. H. Rediker, *J. Appl. Phys.* **1971**, *42*, 2911.
[39] T. Bak, M. K. Nowotny, L. R. Sheppard, J. Nowotny, *J. Phys. Chem. C* **2008**, *112*, 12981.
[40] P. Tiwana, P. Docampo, M. B. Johnston, H. J. Snaith, L. M. Herz, *ACS Nano,* **2011**, *5*, 5158.
[41] S. Chappel, S.-G. Chen, A. Zaban, *Langmuir,* **2002**, *18*, 3336.
[42] S. M. George, *Chem. Rev.* **2010**, *110*, 11.
[43] X. Jiang, K. M. Karlsson, E. Gabrielsson, E. M. J. Johansson, M. Quintana, M. Karlsson, L. Sun, G. Boschloo, A. Hagfeldt, *Adv. Funct. Mater.* **2011**, *21*, 2944.
[44] M. Gorgoi, S. Svensson, F. Schäfers, G. Öhrwall, M. Mertin, P. Bressler, O. Karis, H. Siegbahn, A. Sandell, H. Rensmo, W. Doherty, C. Jung, W. Braun, W. Eberhardt, *Nucl. Instr. and Meth. A* **2009**, *601*, 48.
[45] B. Cheng, J. M. Russell, W. Shi, L. Zhang, E. T. Samulski, *J. Am. Chem. Soc.* **2004**, *126*, 5972.
[46] O. Lupan, L. Chow, G. Chai, H. Heinrich, S. Park, A. Schulte, *Physica E* **2009**, *41*, 533.
[47] W. M. Haynes, 'CRC Handbook of Chemistry and Physics', 92nd Ed. (Internet Version), CRC Press/Taylor and Francis, Boca Raton, US, **2011**.
[48] J. Aarik, A. Aidla, H. Mändar, T. Uustare, *App. Surf. Sci.* **2001**, *172*, 148.
[49] S. Hüfner, 'Photoelectron spectroscopy: Principle and application', Springer-Verlag, Heidelberg, Germany, **2003**, p. 12.
[50] G. G. Fuentes, E. Elizalde, F. Yubero, J. M. Sanz, *Surf. Interface Anal.* **2002**, *33*, 230.
[51] X. Ai, N. A. Anderson, J. Guo, T. Lian, *J. Phys. Chem.* **2005**, *109*, 7088.
[52] C. Bauer, G. Boschloo, E. Mukhtar, A. Hagfeldt, *Int. J. Photoenergy* **2002**, *4*, 17.
[53] J. R. Jenning, L. M. Peter, *J. Phys. Chem. C* **2007**, *111*, 16100.
[54] Y. Diamant, S. G. Chen, O. Melemed, A. Zaban, *J. Phys. Chem. B* **2003**, *107*, 1977.
[55] T. Miyasaka, T. N. Murakami, *Appl. Phys. Lett.* **2004**, *85*, 3932.
[56] M. Wang, P. Chen, R. Humphry-Baker, S. M. Zakeeruddin, M. Grätzel, *Chem. Phys. Chem.* **2009**, *10*, 290.
[57] H. J. Snaith, R. Humphry-Baker, P. Chen, I. Cesar, S. M. Zakeeruddin, M. Grätzel, *Nanotechnology* **2008**, *19*, 424003.
[58] A. Cravino, P. Schilinsky, C. J. Brabec, *Adv. Func. Mater.* **2007**, *17*, 3906.